Regime transitions of granular flow in a shear cell: a micromechanic study

X. Wang[1], H.P. Zhu[2], S. Luding[3] and A.B. Yu[1*]

[1] Laboratory for Simulation and Modeling of Particulate Systems, School of Materials Science and Engineering, University of New South Wales, Sydney, NSW 2052, Australia
[2] School of Computing, Engineering and Mathematics, University of Western Sydney, Locked Bag 1797, Penrith, NSW 2751, Australia
[3] Multi Scale Mechanics, Faculty of Engineering Technology (CTW), MESA+, University of Twente, PO Box 217, 7500 AE Enschede, Netherlands

ABSTRACT

The regime transitions of granular flow in a model shear cell are investigated numerically with a stress-controlled boundary condition. The correlations between elastically/kinetically scaled stresses and packing fraction are examined and two packing fractions (0.58 and 0.50) are identified for the quasi-static/intermediate and intermediate/inertial regime transitions. The profiles and structures of contact networks and force chains among particles in different flow regimes are investigated. It is shown that the connectivity (coordination number) among particles and the homogeneity in the shear flow increase as the system goes through the inertial – intermediate – quasi-static regimes, and there is only little variation in the internal structure after the system has entered the quasi-static regime. Short-range force chains start to appear in the inertial regime, also depending on the magnitude of the shear rate. The percolation of system-spanning force chains through the whole system is a characteristic of the onset of the quasi-static regime, which happens at a packing fraction that is close to the glass transition, i.e. about random loose packing (0.58), but far below the isotropic, quasi-static (a-thermal) jamming packing fraction of random close packing (0.64). The tails of the probability density distribution $P(f)$ of the scaled

* Corresponding author; email: a.yu@unsw.edu.au

normal contact forces for the flows in different regimes are quantified by a stretched exponential, $P(f) = \exp(-cf^n)$, with a remarkable finding that n~1.1 may be a potential demarcation point separating the quasi-static regime and inertial/intermediate regimes.

KEYWORDS: Discrete element method, flow regimes, structural analysis, force network, force statistics

PACS: 45.70.Mg Granular flow: mixing, segregation and stratification; 45.70.Vn Granular models of complex systems; traffic flow; 47.57.Gc Granular flow

1. INTRODUCTION

Granular materials are widely encountered in nature and in industries. The transportation, storage, mixing, fluidization and coating of solid powders are routine processes in industries such as food, mining, chemical and pharmaceutical. In these processes, particulate materials can display very complicated dynamic behavior due to both the complex interactions between constituent particles and their interactions with surrounding gas or liquid and walls [1]. Even though we consider the cases where the interstitial fluid plays an insignificant role and particle-particle interactions are predominant, a general theory of the dynamics of grain flows is still lacking [2]. Complexity in formulating such a theory arises partly from the fact that particle flows can fall into three distinct but interconnected regimes: quasi-static, intermediate and inertial. In the past, many efforts have been dedicated to studying the two ends of the spectrum. On one end, slowly sheared particles are in close contact and the resulting stresses are of quasi-static, rate-independent, Coulomb type. Continuum theory of elasto-plasticity is one of the many possible examples that could be used to model the stresses in this regime [3, 4], but has serious shortcomings with respect to the smooth transition between (almost) elastic and perfectly plastic regimes [5, 6]. On the other end, rapidly flowing assemblies of particles behave inertially and constituent grains are likely to be in contact for a short time. The resemblance of particles in this highly agitated regime to gas molecules leads to that the so-called kinetic theory is used to describe the particle flows in this regime [7-13]. Somewhere in-between the quasi-static and inertial flow regimes, a transitional regime can be identified, which is also called the intermediate regime. The flow characteristics in this regime have been investigated in terms of dense kinetic theory [13]; their frictional-collisional [14-16] or

elastic-inertial [17-19] nature is recognized as one of the most difficult problems in granular materials research [20, 21]. Although various constitutive equations proposed in the literature (see, e.g., [6] and references therein) have achieved a certain extent of success in depicting some aspects of the corresponding regimes, they often become inapplicable when there is a flow regime change.

The understanding of regime transitions and a regime map for granular flows is essential in order to derive an accepted general constitutive relation, which is applicable to all flow regimes. There are a lot of studies concerning phase change in granular flows under two kinds of system-scale constraint: volume- or strain-controlled [17, 22-25], stress-controlled [6, 18, 26] or mixed stress-strain control modes like, e.g. tri-axial tests [5]. The earliest work devoted to granular flow mapping can be attributed to Babic et al. [21]. In their work, they employed a discrete element method (DEM) to simulate a 2D, volume-controlled system of simple shear flow, with inelastic mono-sized disks. They constructed a regime chart in the parametric space of volume fraction – dimensionless shear rate and divided the space into three parts by considering the parameters of coordination number and collision frequency: quasi-static flow, rapid flow and transitional flow. A subsequent and more comprehensive study in this field is due to Campbell [17], who investigated a 3D, volume-controlled system of simple shear flow, with mono-sized, cohesionless and frictional particles. He found four flow regimes: elastic—quasi-static, elastic—inertial, inertial—collisional, and inertial—non-collisional. Since different aspects of granular flow were examined in the determination of flow regimes, the regime charts due to Babic et al [22] and Campbell [17] reflected different fundamental physics. Campbell [18] attempted to link the two regime charts, and found that the quasi-static regime in [22] did not correspond to any regime in [17] as the densities considered were totally

different. Considering both volume-controlled and stress-controlled cases, Campbell [18] compared the results from both cases and drew the conclusion that there were significant differences between these two types of systems and that rheological properties obtained in volume-controlled system might not be applied to stress-controlled systems or vice versa. However, this issue was closely examined and put in doubt later by Aarons and Sundaresan [23, 26]. They investigated both volume-controlled and stress-controlled systems of simple shear flow with mono-sized, spherical and cohesive particles, and found that the rheological behavior of particles was the same regardless of whether the system was stress-controlled or volume-controlled, and thus the regime map was independent of the type of the system constraint. In a subsequent paper by Campbell [27], the rheology of ellipsoidal particles under volume controlled conditions was studied but the difference between the two boundary conditions was not addressed.

Despite the useful conclusions drawn from these studies, there is still no consensus regarding how an entire flow regime map can be drawn and if a change in the system-scale constraint has an influence on the regime map. Of the two types of constraint, the stress-controlled condition is more relevant in reality as there is always free space in which granular flow can expand or compress in response to different stresses and particles always have to support a certain amount of overburden. Exceptions are flows with a free surface [6], where the particles experience no confining stress – however, this extreme case will not be considered in this work. In addition, even though the quasi-static regime has been studied in detail [6, 28], there is no complete picture on the structures in different flow regimes, which can offer deep insights into the underlying physics of these regimes. Only recently the concept of structural anisotropy

has been added to constitutive models as it represents a microscopic measure for the deformation history (see [5, 25, 28] and references therein).

In the present study, we present a 3D DEM simulation to examine regime transitions in a stress-controlled model shear cell, one of the simplest practical devices in testing the rheological properties of granular materials [30-32]. The main issues we will address in this work include: (a) the determination of regime transitions in granular flow, and (b) the evolution of internal structures as the system goes through regime transitions. To the authors' knowledge, the second aspect has hardly been touched in the literature. The connection between the microscopic structure and flow regimes will be examined as part of this study. In particular, the regime below the jamming transition, which has only recently received experimental attention in the slow, quasi-static limit [33], will be studied at different shear rates. The findings can offer some insights into the dynamical characteristics for different flow regimes.

2. SIMULATION METHOD

2.1 DEM approach

In the present work, a DEM approach [34] is used to simulate granular flow in a rectangular cell, resembling large radius annular shear cells. In such a simulation, a particle has two types of motion: translational and rotational, described by Newton's laws of motion. Since fine particles are not involved, and air and moisture are not present here, forces other than mechanical contacts, e.g., particle–fluid interaction forces, can be neglected. As a result, the governing equations for the translational and rotational motion of particle i with mass m_i and moment of inertia I_i can be written as

$$m_i \frac{d\boldsymbol{v}_i}{dt} = \sum_j \boldsymbol{F}_{ij}^{\,c} + \boldsymbol{F}_i^{\,g} \tag{1}$$

$$I_i \frac{d\boldsymbol{\omega}_i}{dt} = \sum_j \boldsymbol{M}_{ij} \tag{2}$$

where $\boldsymbol{v}_i$ and $\boldsymbol{\omega}_i$ are the translational and angular velocities of the particle, $\boldsymbol{F}_{ij}^{\,c}$ and $\boldsymbol{M}_{ij}$ are the contact force and torque acting on particle i by particle or wall j, and $\boldsymbol{F}_i^{\,g}$ is the gravitational force. The contact force is comprised of a (non-linear, Hertzian) elastic contact force and a damping contribution. As for the torque ($\boldsymbol{M}_{ij}$) acting on particle i, a rolling friction torque is also included in addition to the torque generated by the tangential force on the particle. The rolling friction torque is generated by asymmetric normal forces and slows down the relative rotation between particles. The details on the models for contact force and torque can be seen elsewhere (e.g., [35, 36]). The models used here have been successful in exploring the fundamentals of various systems (see [1] and references therein).

2.2 Simulation conditions

The configuration of a typical annular shear cell is shown in Fig. 1 (a), which is similar to the one considered in our previous studies [37, 38]. Here, to improve computational efficiency, only a flat, rectangular segment of the shear cell is simulated (Fig. 1 (b)) and periodic boundary conditions are used to represent the symmetrical geometry of the whole annular space. Note that the circumferential curvature is ignored in this setting. However, the key operational features of the shear cell are still maintained. This simplification has also been used by other investigators to study other aspects of annular shear cells [39, 40]. The cell consists of an upper platen and a lower platen (perpendicular to the Z-axis and with a uniform dark color in Fig. 1 (b)), two

stationary walls (perpendicular to the Y-axis and with a dark shaded color in Fig. 1 (b)) and two periodic boundary planes (perpendicular to the X-axis). Both the upper and lower platens of the cell are formed by 360 glued spherical particles that have the same size and material properties as the flowing particles. This sheared granular material in the cell consists of 5,000 spherical particles with a diameter of d. The cell dimensions are 12d and 30d in X- and Y- directions, respectively, the same as those used in our previous studies [38]. The shear velocity of the platens and the normal stress applied in the negative Z-direction were precisely controlled. Trial tests indicate that a larger cell does not affect much the results (data not shown for brevity).

For each simulation, the 5,000 spherical particles were first generated randomly, and then discharged at a pre-set rate from the top without the upper platen. After a certain period of time, the particles formed a packing on the lower platen. The upper platen was then placed on the top of the packing. Using a gravitational time-scale as the unit of time, from $t = 40.0\sqrt{d/g}$, the lower platen was given a gradually increasing shear velocity in the positive X-direction, and the upper platen was given both a gradually increasing shear velocity in the negative X-direction and a gradually increasing normal stress in the negative Z-direction. At $t = 70.0\sqrt{d/g}$, the velocities and normal stress reached the pre-set target values. From then the bulk properties of the system were closely monitored. If these properties only showed minor fluctuations around constant values, then the system was assumed to be in steady state. It was observed that the shearing systems quickly became steady. Consequently, at $t = 80.0\sqrt{d/g}$, the process of calculating microstructural and dynamic properties started and was carried out until the simulations finished at $t = 160.0\sqrt{d/g}$.

Following the approach of Campbell [17, 18], scaled physical properties were adopted in this work, including elastically scaled stress $\sigma^*=\sigma d/k$, kinetically scaled stress $\sigma'=\sigma/\rho d^2\dot{\gamma}^2$ and scaled stiffness $k^*= \sigma'/\sigma^*=k/\rho d^3\dot{\gamma}^2$, where σ is the applied normal stress, ρ is particle density, d is particle diameter, $\dot{\gamma}$ is the effective shear rate due to the platens and k is the material stiffness. The physical meaning of σ^* is the particle deformation induced by the applied stress, relative to its size [17, 18]. The scaled physical parameters vary while other parameters are kept constant. The packing fraction will be used as a key parameter to study the regime transition. The simulations showed that the fluctuations of the cell height were less than 1% of its average value after the flows reached their macroscopically steady state for the cases considered. This indicates that the packing fraction has little variation in the steady state To eliminate the effect of the fluctuation, the packing fraction for each case is averaged from $t=80.0\sqrt{d/g}$ to $t=160.0\sqrt{d/g}$, in which the flow is considered to be in the steady state. The input and output parameters and their values are listed in Table 1. The material stiffness k was estimated by $k=(8/3)ER$, where E is the effective Young's Modulus, defined as $1/E=2(1-\alpha^2)/E_0$, and α and E_0 are the Poisson ratio and Young's modulus of particles, respectively. R is the effective radius, defined as $1/R=2/R_0$, where $R_0 = d/2$ is the radius of the particles [41]. Our focus in this work is to understand the physics of the flow regimes and regime transitions from the viewpoint of structural evolution. So, the range of the scaled parameters in this work is not as extensive as those used in the previous studies [17, 18, 23, 24, 26].

3. RESULTS AND DISCUSSION

In this section, we will first consider the determination of regime transitions, which are controlled by varying the values of shear rate and applied pressure. The variation of the internal structure is then examined in relation to the regime transitions. Finally, the corresponding distribution of the normal forces among particles is analyzed.

3.1. Determination of regime transitions

Fig. 2 shows the dependence of the elastically scaled applied stress (σ^*) on packing fraction (ν) for different values of the scaled stiffness (k^*). When there is no inertial effect in the system (quasi-static regime), particles are confined by their neighbours and only interact elastically. In this case, the particle deformation only depends on the applied stress. As the system constraint (applied normal stress) is relaxed, inertial effects become increasingly significant, and the particle deformation is more and more sensitive to the shear rate. Fig. 2 shows that when $\nu \geq 0.58$, the data corresponding to different values of k^* tend to collapse into one master curve, indicating that the elastically scaled stress of the dense systems is independent of k^* (shear rate) in the quasi-static regime. For $\nu < 0.58$, the data for different k^* start to deviate from each other, implying the appearance of inertial effects. As a result, $\nu = 0.58$ is a critical packing fraction that separates the quasi-static and intermediate regimes, lower than 0.65 as determined in [24]. A possible reason is that the existence of two stationary walls perpendicular to the Y-direction facilitates the formation of force chains in the present work, while there are no walls in the system in [24].

In order to determine the transition between the intermediate flow and inertial flow, we employed the same method used by Ji and Shen [24] and Aarons and Sundaresan

[26]. The method involves identifying the correlation between kinetically scaled stress $\sigma'=\sigma/\rho d^2\dot{\gamma}^2$ and packing fraction ν. According to Campbell [18], the stresses are proportional to the product of transported momentum and transport rate for particles. For inertial flows, both the transported momentum and transport rate are proportional to the shear rate. As a result, the stresses scale quadratically with shear rate in the inertial regime, so that the kinetically scaled stress $\sigma'=\sigma/\rho d^2\dot{\gamma}^2$ can be used to identify the inertial regime. The results from this scaling are shown in Fig. 3. It is observed that the data collapse below ν = 0.50, but when the packing fraction is high (e.g. $\nu \geq 0.58$), the data of σ' for different values of *k** demonstrate significant differences, showing that the kinetically scaled stress is greatly dependent on k* for shear rates in the quasi-static regime. This indicates that the stress for all the flows scales kinetically with packing fraction below a threshold density and thus the flows are in the inertial regime. The same data collapse behavior and dependence of σ* and σ' on ν can also be observed in volume-controlled systems [17, 24]. Thus we are able to show that the rheological properties of granular flows under volume- and stress-controlled conditions are actually the same, as suggested by Aarons and Sundaresan [26].

Different *k** values were used in Figs. 2 and 3. Similar to the treatment of Aarons and Sundaresan [26], we can determine the regime transition sets of (σ*, *k**) and (σ', *k**). The points close to the lines ν = 0.58 and ν = 0.5 in Figs 2 and 3 are considered as the quasi-static/intermediate and intermediate/inertial regime transition points respectively. Correspondingly, (σ*, *k**) = (6×10^{-2}, 2.5×10^{5}), (6×10^{-2}, 3×10^{4}), (6×10^{-2}, 3×10^{3}) and (6×10^{-2}, 3×10^{2}), and (σ', *k**) = (14841.24, 2.5×10^{5}), (1623.16, 3×10^{4}), (180.35, 3×10^{3}) and (20.00, 3×10^{2}) were obtained for the quasi-static/intermediate regime transition, while (σ*, *k**) = (9×10^{-6}, 2.5×10^{5}), (1.5×10^{-4}, 3×10^{4}), (6×10^{-4}, 3×10^{3}) and (6×10^{-3},

3×10^2) and (σ', k*) = (2.226, 2.5×10^5), (4.058, 3×10^4), (1.804, 3×10^3) and (2.000, 3×10^2) are for the intermediate/inertial regime transition.

With all the transition points determined above, we are able to obtain a flow regime map. Fig. 4 (a) shows the regime map in the parametric space of (σ*, k*). On one hand, if k* (shear rate) is fixed, the decrease of σ* causes the system to change from quasi-static to intermediate, and finally to inertial regime. This is reasonable because for a given shear rate, decreasing the applied stress reduces the constraint on the system, allowing the system to expand. On the other hand, when σ* (applied stress) is fixed and very large, the system always stays in the quasi-static regime no matter what value the shear rate is, i.e. there is no path between quasi-static and intermediate regimes in the parametric space of (σ*, k*) for fixed σ*. For lower σ*, the system contact constraints are mitigated so that particles can exhibit inertial effects as the shear rate becomes larger (k* becomes smaller), i.e. the particles become more agitated and the system goes through the transition from intermediate regime to inertial regime.

We can also draw the regime map in the parametric space of (σ', k*) as shown in Fig. 4 (b). The results in the figure indicate that the system changes from the quasi-static to intermediate, and finally to inertial regime, when the shear rate is fixed and the applied stress (σ') is lowered. Another important feature is that when σ' is low enough, the system always stays in the inertial regime. This is understandable since σ' by definition is the ratio of elastic stress (force chain intensity, as discussed below) and kinetic energy in the system. A small value of σ' indicates that particles in the system are highly agitated, which is naturally the characteristic of the inertial regime. As σ' becomes larger, large scale force chains become increasingly predominant. In this case, for a fixed σ', the decrease in k* (or the increase in shear rate) will make the system

transit from the intermediate to the quasi-static regime due to the increased applied pressure (or particle deformation). Note that the developing trend of the borderlines between two regimes would change if k^* is out of the range considered in Fig. 4. More detailed information can be seen in [18]. Furthermore, only one of the two regime plots is unique, since they are connected via the definition of $k^* = \sigma'/\sigma^*$.

We have also considered the effect of particle material properties, including sliding friction, rolling friction and normal restitution coefficient, on the features considered above. These properties do not much affect the qualitative trends of σ^* and σ' with v, but they have an influence on the values of the critical packing fraction for the regime transitions. For example, an increasing sliding friction coefficient decreases both critical packing fractions for the quasi-static/intermediate and intermediate/inertial regime transitions. Increasing rolling friction lowers the value of v for the transition into the quasi-static regime, while the increase in restitution coefficient boosts the value for the intermediate/inertial regime transition. Such issues will be discussed in another paper in more detail.

3.2 Structural analysis

In order to qualitatively examine the structure of the studied shear flows, we first look at the contact networks under different conditions of (σ^*, k^*). It should be noted that as the variation in the magnitude of normal force is huge for different cases in the present work, it is inconvenient to compare the normal force networks using a universal scaling (typical examples of normal force networks can be found in [28,43-45]). As a consequence, we plot the networks of scaled normal forces (f), which is defined as the ratio of normal contact forces (F_n) to the average normal contact force ($\langle F_n \rangle$) for a specific case, i.e. $f = F_n/\langle F_n \rangle$. In this way, we can compare the network or

connectivity profiles of different cases using the same scale. In the contact network diagrams of the present work, each stick represents a line joining the centres of two contacting particles and its thickness stands for the magnitude of the scaled normal contact force between them. To be illustrative, and to avoid artefacts to the vicinity of walls, the figures are constructed based on the particles in the central slice (2*d* in thickness) along the shear (x-axis) direction.

Fig. 5 shows the contact force networks for $k^*=3\times10^2$ and eight different values of σ*, together with the corresponding packing fractions and average coordination numbers. The average coordination number is the bulk average for all the sheared particles in the system. In Fig. 5 (a), σ* takes a relatively low value of 3×10^{-4} and the system is in the inertial regime, i.e. relatively dilute with packing fraction 0.32. An average coordination number of 1.45 means that multi-particle contacts are infrequent and connectivity among particles is very low. Scaled contact forces of both high and low magnitudes exist in the system, implying the high heterogeneity of the force network in the inertial regime. As σ* increases to 6×10^{-3} (Fig. 5 (c)) via the value of 3×10^{-3} (Fig. 5 (b)), the system goes through the inertial regime and reaches the boundary between the inertial and intermediate regimes. The connectivity among particles increases as manifested by the increase in coordination number from 1.45 to 3.42 due to the increasing system constraint and the resultant growth in packing fraction. It is also noticed that there is an increasing number of weak scaled contact forces in the background, implying that their percentage increases in the process, while that of the strong scaled forces is diminishing. The system enters the intermediate regime as σ* increases beyond 6×10^{-3}, for example, to 1.5×10^{-2} (Fig. 5 (d)) and 3×10^{-2} (Fig. 5 (e)). The characteristic of this stage is that the internal structure becomes more and more closely knit, which is manifested by the steady increase in the average coordination

number from 3.42 to 4.79. In addition, both the relatively infrequent appearance of the large scaled forces and the stronger background of the weak forces indicate that the system considered becomes more dense and homogeneous. After σ^* increases above the boundary value of 6×10^{-2} (Fig. 5 (f)), the system starts to enter the quasi-static regime. Figs. 5 (g) and (h) demonstrate the contact networks when $\sigma^*=0.15$ and 0.3, respectively. Note that in the quasi-static regime, there seems to be little visible variation in the dense internal structure despite an increase in connectivity, implying the high stability of the internal structure of quasi-static flows. For a more quantitative analysis of the contact network under different densities in the inertial and quasi-static regimes, see Refs. [25, 29] and references therein.

We compare our results with the contact force networks of a simple shear flow in different flow regimes reported in [18] and find that the agreement is apparent despite the fact that the contact forces in [18] are not scaled by their average in each case. The networks shown in Figs. 5 (a), (d) and (e) in the present work are consistent with the collisional and elastic-inertial networks reported in Figs. 2 (d), (c) and (b) in [18], respectively. The quasi-static networks shown in Figs. 5 (g) and (h) in this work also agree well with their counterpart in Fig. 2 (a) in [18]. This agreement implies that there are some universal features of granular flows in the same flow regime, even if the flows have different configurations or boundary conditions.

The research on force chains has been a very important component in the demarcation and characterization of different flow regimes (see [46] for example). It has been reported that the parts where there are no force chains can be associated with the existence of inertial effects [42]. In this work, we examine the characteristics of force chains (if any) for different flow regimes for the considered systems. To this end,

following the work of Peters et al. [46], we define a force chain as a quasi-linear particle assembly where stress is concentrated; concentrated stress means that the contact forces with magnitudes greater than the average form connected force chains. Therefore, we remove, from Fig. 5, the scaled contact forces (f) with magnitudes less than or equal to one, where the cut-off is an arbitrary but convenient/simple choice. The remaining scaled forces satisfy the condition of $f>1$, i.e. $F_n > \langle F_n \rangle$. For brevity, only four cases corresponding to Figs. 5(a), (b), (d) and (e) are plotted in Fig. 6. Note that the quantitative examination of the 'quasi-linear' and 'particle assembly' conditions is beyond the scope of this work, but we can provide some qualitative descriptions here.

Figs. 6 (a) and (b) depict the structure of large scaled forces ($f>1$) in the inertial regime. The difference is that the case in Fig. 6 (b) is closer to the boundary between inertial and intermediate regimes. The main interaction mode in Fig. 6 (a) are binary collisions, with no strong, concentrated force chains formed in the system. This clearly corresponds to the traditional rapid flow or the inertial-collisional regime reported in [17-19]. In Fig. 6 (b), the particle interactions become more frequent than those in Fig. 6 (a). Some local contact clusters or chains appear, implying that the flow could be in the so-called inertial-noncollisional regime reported in [17-19]. According to Campbell [17-19], particles should break free from force chains in the inertial regime so there are no significant long force chains in this regime. However, we find that there are some (temporary) short-range force chains with three to four stress-bearing particles in the inertial regime in Fig. 6 (b). Therefore, the inertial-noncollisional regime may include not only particle clusters but also short force chains for some cases. In Fig. 6 (c), one can find that system-spanning force chains start to form in the intermediate regime with respective increase in connectivity and packing fraction.

Considering the force chains are short in the inertial flow, we may conclude that the appearance of system-spanning force chains, instead of the short force chains in granular flows with high shear rates, can be used as an indication of the emergence of quasi-static effects. As σ* increases further, the number of the system-spanning force chains grows and inertial domains (i.e. no force chains) are gradually 'squeezed' out of the system. When the inertial effects disappear with the application of higher normal stresses, the system enters the quasi-static regime as shown in Fig. 6 (d), which is characterized by the percolation of system-spanning force chains through the whole cell [33].

At this point, we should remark that Campbell [18] proposed a different method to determine the quasi-static/intermediate regime transition points. According to his method, the points where the data for different k^* deviate from the critical state (or transition) are considered as the indicators of the quasi-static/intermediate regime transition. This method is not suitable for some cases considered here, as demonstrated in the examination of the relevant force chains. Fig. 6 (c) belongs to the intermediate regime according to the flow chart drawn in Fig. 4 (a), and it is also in the low stress critical state [18] as shown in Fig. 2. According to the criterion in [18], Fig. 6 (c) would belong to the quasi-static regime since its corresponding point in the (ν, σ*) space in Fig. 2 does not deviate from the critical state line. However, the strong scaled force network in Fig. 6 (c) clearly shows that the system-spanning force chains have not percolated the whole system yet and some part of the cell space is still dominated by inertial domains (with no force chains formed), implying that the flow is in the intermediate regime.

3.3 Force statistics

The force network among particles in a static or dynamic state can be analyzed in terms of the force probability distribution, which can give us some hints regarding the general behavior of granular systems [28, 47]. Many studies have been devoted to determining the shape of the probability density distribution of the normal contact forces between particles, $P(f)$, and its variation under different conditions [48-51], in addition to the long range correlations in the forces [28]. Efforts have also been made to investigate the signature change in $P(f)$ when systems go through jamming transitions [51-53]. In this work, we use similar ideas to determine if there is any change in the shape of $P(f)$ as the granular flow changes between different flow regimes. Note that due to shear and the consequent anisotropy the orientation-angle of the contact forces is important for the analysis of two-dimensional force distributions (see [54] and references therein). This complicated issue in three dimension will be considered in our future study.

The probability distributions of the scaled normal contact force, f ($=F_n/\langle F_n \rangle$), for flows under different conditions are shown in Fig. 7. In general, the distribution becomes wider as the flow goes through the quasi-static – intermediate – inertial regime transitions. In the quasi-static regime, the force distributions obtained in the present work have a similar trend to those for static packings obtained in [28, 48, 49]. The force chains percolate the whole system and the majority of particles contribute to the network bearing large forces as, for example, shown in Fig. 6 (d). At the same time, the average normal force <Fn> is large (see the insets of Fig. 7 for the variation of <Fn>), and the distribution is relatively even. In the intermediate and inertial regimes, the force chains gradually disappear and an increasing number of particles interact by

collisions. The examples of the force networks in the inertial regime can be seen in Figs. 6 (a) and (b). Only a limited number of collisions are noticeable and most interactions are fairly weak, resulting in a very small $<F_n>$ (the insets of Fig. 7). As a result, the corresponding scaled force distribution is rather wide.

In Fig. 7, we include the force distributions corresponding to the boundary points of quasi-static/intermediate (B_{qi}) and intermediate/inertial (B_{ii}) transitions. Although the distributions vary for B_{ii} under different values of k^*, they remain invariant for B_{qi}. This is confirmed for many other values of k^* (data not shown for brevity). That is, the force distributions of the granular flows under different shear rates share a common feature when they go through the quasi-static/intermediate transition. The tails (large f range) of the force distributions can be fitted by a stretched exponential:

$$P(f) = \exp(-cf^n) \tag{3}$$

where c and n are fitting parameters. This functional form is consistent with the one in [28,49]. In this work, the best-fitting values of n close to the inertial/intermediate and intermediate/quasi-static regime boundaries are examined in terms of its correlation with ν, as shown in Fig. 8. It is observed that the best fitting to the force distributions of B_{qi} under different k^* corresponds to n=1.1 with typical variation/uncertainty of 0.05 Using n=1.1 as a demarcation point, n>1.1 is for a flow in the quasi-static regime and a higher value of n means the flow is deeper into the quasi-static regime; n<1.1 corresponds to a flow in the intermediate or inertial regime and a lower n signifies larger inertial effects. We note that this is a remarkable common feature in the force distributions for all the considered flows at different k^*, and one can tell if there is any significant inertial component in a granular flow from the tail of its force distribution. Therefore, the value of n can potentially serve as an alternative indicator for the

emergence of the quasi-static regime.

3.4 Coordination number in regime transitions

In this section, we try to quantitatively explain why the demarcation between the quasi-static and intermediate regimes works from the micro-dynamic perspective. Fig. 9 (a) shows the variation of coordination number (*CN*) with packing fraction (ν) for different scaled stiffness k^*. The data can be categorized into two groups, divided by a demarcation point corresponding to $\nu = 0.58$ with a critical coordination number of around 5.6 (which is close to the isostatic point 6.0). In the first group where $\nu < 0.58$, *CN* increases with the decrease of k^* (or the increase of shear rate) for a given ν; while in the second group where $\nu > 0.58$, the variation of *CN* with ν is independent of k^* and the data of *CN* collapse more or less. The first group belongs to the flow regimes in which inertial effects play an obvious role and any increase in shear rate enhances particle contacts; the flow characteristics are hence influenced by the shear rate (i.e. k^*). As a result, the data in the first group should be in the intermediate or inertial regimes. For the second data group, the fact that the increase in shear rate cannot cause any change in particle contacts indicates that the force chains have percolated the whole system. Naturally, the corresponding systems are practically rate-independent and thus belong to the quasi-static regime.

In Section 3.1, we showed that the data of σ^* collapse when ν exceeds the same critical packing fraction (0.58). As a result, one would expect that there should also be a data collapse between *CN* and σ^* when *CN* is higher than its critical value (~5.6). To test this speculation, we plot the correlation between *CN* and σ^* for different k^* in Fig. 9 (b). As expected, the data pattern presented in this figure is highly similar to that in Fig. 2 and the data for *CN* and σ^* collapse when *CN* exceeds ~5.6. Therefore, it is also

feasible to use the correlation between *CN* and σ* to determine the intermediate/quasi-static regime boundary. For the correlation between *CN* and σ', there is no such collapse, as indicated in Fig. 9 (c), neither for the inertial, nor for the quasi-static regime.

In Section 3.2, we showed that as the flows enter the quasi-static regime, the force chains percolate through the whole system and all the particles in the system are tightly confined in the contact network as observed in Figs. 5 (g)-(h) and Fig. 6 (d). This phenomenon is reminiscent of global jamming in granular packings [55] and strongly resembles the observations of jamming under shear [33]. The packing fraction (0.55), corresponding to the onset of global jamming [55], appears close to the one (0.58) for the quasi-static/intermediate transition in the present study. However, changes in packing fractions as small as 0.03 can lead to enormous changes in CN and even more in σ*, so that one has to be careful when defining differences in jamming packing fractions [25, 28]. It would be of interest to examine further if and how global jamming is truly related to this regime transition.

The concept of jamming has long been used to describe the transition to rigidity of a series of disordered materials such as foams, granular matter and glasses [56, 57]. The behavior of materials near and above the jamming transition is extensively studied with regard to the correlation between average coordination number and packing fraction, while much less attention has been given to the regime below jamming [33]. It is found that, both experimentally and numerically, a granular system going through a global jamming transition exhibits the following two attributes [58-64]: (a) the average coordination number *CN* of the system increases sharply at the transition point when increasing the packing fraction *v* above a certain value ν_0 (see [28] and

references therein), and (b) *CN* still increases as a function of $\Delta\nu$ ($\Delta\nu=\nu-\nu_0$) above ν_0, with the transition point defined as (ν_0, CN_0). Both attributes are suspect to finite size effects and have to be considered very carefully.

For frictionless spheres [28, 58-61], a simple scaling feature exists above the jamming transition point in the form of $CN-CN_0 = (\nu-\nu_0)^{\beta}$, where $\beta \sim 0.5$, while for frictional particles, different values of ν_0 and CN_0 are identified with very similar values of β. More recently, Imole et al. [25] reported that the jamming transition packing fraction is also a function of the applied deformation mode, but they also confirmed that the scaling holds almost perfectly, while it is independent of force laws [62]. To check the scaling law in the present sheared system, we plot $CN-CN_0$ against $\nu-\nu_0$ in the inset of Fig. 9 (a) (ν_0 and CN_0 are 0.58 and 5.6 respectively). We can see that the data collapse (except for the smallest k^*), indicating that the flow becomes globally jammed when ν is larger than 0.58, the demarcation point for the quasi-static/intermediate transition. We can get the best fit for the data points as $\Delta CN=14.021\Delta\nu-21.007(\Delta\nu)^2$, where $\Delta CN= CN-CN_0$ and $\Delta\nu= \nu-\nu_0$, with a correlation coefficient of 0.992. Thus, the correlation between $CN-CN_0$ and $\nu-\nu_0$ takes a quadratic form in the present granular flows, instead of a square root form found in the static granular packing [58-62]. This may be attributed to the fact that, although the structural change in the present system can be analyzed in terms of global jamming transition, dynamic granular flow may be very different from static granular packings.

4. CONCLUSIONS

The shearing of particles in a model shear cell under stress-controlled conditions has been investigated numerically using the discrete element method. Granular flows under different conditions of scaled stiffness ($k^*=k/\rho d^3\dot{\gamma}^2$) and scaled normal stress

($\sigma^*=\sigma d/k$) are considered, and packing fraction (ν) and kinetically scaled stress ($\sigma'=\sigma/\rho d^2\dot{\gamma}^2$) for each flow are calculated. The data collapse between σ^* and ν for different k^* when $\nu > 0.58$ is considered as lower limit packing fraction of the quasi-static regime, while the data collapse between σ' and ν for different k^* when $\nu < 0.50$ is deemed as the indication (upper limit) of the inertial regime. This regime demarcation method of identifying two critical packing fractions is consistent with that used in [24], but different from that using the low stress critical state [18].

The internal structures of the flows in different regimes (quasi-static/intermediate/inertial) have been investigated concerning the evolution of contact networks and force chains for different combinations of σ^* and k^*. The results show that the different attributes of the three flow regimes and the corresponding transitional behaviors can adequately be reflected in the contact networks or force chains, together with the information about average coordination number and packing fraction. A striking result found here is that, contrary to common belief, short-range force chains are observed in the inertial regime for large shear rates. The implication of this finding for the inertial (transitional) regime is that such a flow may contain not only particle clusters as shown by Campbell in [18] but also short or localized force chains. Furthermore, the percolation of system-spanning force chains is a characteristic of the quasi-static regime.

The force statistics analysis shows that the force distribution becomes increasingly wide as the flow transits from the quasi-static to the inertial regime, a phenomenon also observed in thermal systems when temperature increases. The tail of the probability density distribution of scaled normal forces can be well approximated by the form $P(f)=\exp(-cf^n)$. The power index n may serve as a new flow regime

indicator, with n>1.1 for the quasi-static regime and n<1.1 for the intermediate and inertial regimes. This critical n may vary with material properties, which should be studied in the future.

The correlation between coordination number CN and packing fraction ν, is established to testify the robustness of the present demarcation method. It is found that the dependence of CN on σ* can also be used to identify the quasi-static/intermediate regime transition since the same data collapse happens as that between CN and ν. By examining the correlation between CN and ν, we confirm, as observed earlier in quasi-static situations [25, 60], that the transition to the quasi-static regime is related to the global jamming transition. A square-root scaling between ΔCN (=CN-CN0) and Δν (= ν-ν0) also exists for the present sheared system. This result indicates that, although granular shear flows can differ from granular packings in many ways, the snapshots and the averaged (isotropic) properties of their internal structures are comparable. They may share some common characteristics, which should be further explored in future studies, especially concerning anisotropy [25].

Acknowledgements

The authors are grateful to the Australian Research Council and the University of New South Wales for the financial support of the present work. SL especially appreciates a visiting fellowship award by UNSW for his research-visit in June and July 2013.

References

1. H.P. Zhu, Z.Y. Zhou, R.Y. Yang, and A.B. Yu, "Discrete particle simulation of particulate systems: A review of major applications and findings," Chemical Engineering Science **63**, 5728 (2008).

2. Anonymous, "So much more to know," Science **309**, 78 (2005).

3. A. Schofield, and C.P. Wroth, Critical State in Soil Mechanics (McGraw-Hill, New York, 1968).

4. R.M. Nedderman, Statics and Kinematics of Granular Materials (Cambridge University Press, Cambridge, England, 1992).

5. S. Luding, "Anisotropy in cohesive, frictional granular media," J. Phys.: Condens. Matter **17**, S2623-S2640 (2005).

6. S. Luding, and F. Alonso-Marroquin,"The critical-state yield stress (termination locus) of adhesive powders from a single numerical experiment," Granular Matter 13(2), 109-119 (2011).

7. S.B. Savage, and D.J. Jeffrey, "The stress tensor in a granular flow at high shear rates," Journal of Fluid Mechanics **110**, 255 (1981).

8. J.T. Jenkins, and S.B. Savage, "A theory for the rapid flow of identical, smooth, nearly elastic, spherical particles," Journal of Fluid Mechanics **130**, 187 (1983).

9. C.K.K. Lun, S.B. Savage, D.J. Jeffrey, and N. Chepurniy, "Kinetic theories for granular flow: inelastic particles in Couette flow and slightly inelastic particles in a general flowfield," Journal of Fluid Mechanics **140**, 223 (1984).

10. C.K.K. Lun, and S.B. Savage, "The effects of an impact velocity dependent coefficient of restitution on stresses developed by sheared granular materials.," Acta Mechanica **63**, 15 (1986).

11. C.S. Campbell, "The stress tensor for simple shear flows of a granular material.," Journal of Fluid Mechanics **203**, 449 (1989).

12. C.K.K. Lun, "Kinetic theory for granular flow of dense, slightly inelastic, slightly rough spheres.," Journal of Fluid Mechanics **233**, 539 (1991).

13. J. T. Jenkins and D. Berzi, "Kinetic theory applied to inclined flows," Granular

Matter **14**, 79–84 (2012).

14. GDR MiDi, "On dense granular flows," European Physical Journal E **14**, 341 (2004).

15. O. Pouliquen, and F. Chevoir, "Dense flows of dry granular material.," Comptes Rendus Physique **3**, 163 (2002).

16. G.I. Tardos, S. McNamara, and I. Talu, "Slow and intermediate flow of a frictional bulk powder in the Couette geometry," Powder Technology **131**, 23 (2003).

17. C.S. Campbell, "Granular shear flows at the elastic limit," Journal of Fluid Mechanics **465**, 261 (2002).

18. C.S. Campbell, "Stress-controlled elastic granular shear flows," Journal of Fluid Mechanics **539**, 273 (2005).

19. C.S. Campbell, "Granular material flows – An overview," Powder Technology **162**, 208 (2006).

20. M. Massoudi, and T.X. Phuoc, "Conduction and dissipation in the shearing flow of granular materials modeled as non-Newtonian fluids," Powder Technology **175**, 146 (2007).

21. Y. Forterre, and O. Pouliquen, "Flows of dense granular flow," Annual Review of Fluid Mechanics **40**, 1 (2008).

22. M. Babic, H.H. Shen, and H.T. Shen, "The stress tensor in granular shear flows of uniform, deformable disks at high solids concentrations," Journal of Fluid Mechanics **219**, 81 (1990).

23. L. Aarons, and S. Sundaresan, "Shear flow of assemblies of cohesive and non-cohesive granular materials," Powder Technology **169**, 10 (2006).

24. S. Y. Ji, and H. H. Shen, "Internal parameters and regime map for soft polydispersed granular materials," Journal of Rheology **52**, 87 (2008).

25. O. I. Imole, N. Kumar, V. Magnanimo, and S. Luding, "Hydrostatic and Shear Behavior of Frictionless Granular Assemblies under Different Deformation Conditions," KONA **30**, 84-108 (2013).

26. L. Aarons, and S. Sundaresan, "Shear flow of assemblies of cohesive granular

materials under constant applied normal stress," Powder Technology **183**, 340 (2008).

27. C. S. Campbell, "Elastic granular flows of ellipsoidal particles," Physics of Fluids **23**, 013306 (2011).

28. M. K. Müller, T. Pöschel, and S. Luding, "Force Statistics and Correlations in Dense Granular Packings," Chemical Physics **375**, 600-605 (2010).

29. J. Sun, and S. Sundaresan, "A constitutive model with microstructure evolution for flow of rate independent granular materials." Journal of Fluid Mechanics, **682**, 590-616 (2011).

30. S. B. Savage, and M. Sayed, "Stresses developed by dry cohesionless granular materials sheared in an annular shear cell," Journal of Fluid Mechanics **142**, 391 (1984).

31. D. M. Hanes, and D.L. Inman, "Observation of rapidly flowing granular-fluid materials," Journal of Fluid Mechanics **150**, 357 (1985).

32. S. S. Hsiau, and W.L. Yang, "Stresses and transport phenomena in sheared granular flows with different wall conditions," Physics of Fluids **14**, 612 (2002).

33. D. Bi, J. Zhang, B. Chakraborty, and R. P. Behringer, "Jamming by shear." Nature **480**(7377), 355- 358 (2011).

34. P. A. Cundall, and O.D.L. Strack, "A discrete numerical model for granular assemblies," Geotechnique **29**, 47 (1979).

35. H. P. Zhu, Z.Y. Zhou, R.Y. Yang, and A.B. Yu, "Discrete particle simulation of particulate systems: Theoretical developments," Chemical Engineering Science **62**, 3378 (2007).

36. H. P. Zhu, and A.B. Yu, "The effects of wall and rolling resistance on the couple stress of granular materials in vertical flow," Physica A **325**, 347 (2003).

37. X. Wang, H.P. Zhu, and A.B. Yu, "Microdynamic analysis of solid flow in a shear cell," Granular Matter **14**, 411 (2012).

38. X. Wang, H.P. Zhu, and A.B. Yu, "Flow properties of particles in a model annular shear cell," Physics of Fluids, **24**, 053301 (2012).

[39] A. Hassanpour, Y. Ding, and M. Ghadiri, "Shear deformation of binary mixtures of dry particulate solids," Advanced Powder Technology **15**, 687 (2004).

[40] Z. Ning, and M. Ghadiri, "Distinct element analysis of attrition of granular solids under shear deformation," Chemical Engineering Science **61**, 5991 (2006).

[41] H. Hertz, "Über die Berührung fester elastischer Korper," Journal für die Reine und Angewandte Mathematik **92**, 156 (1882).

[42] E. Aharonov, and D. Sparks, "Rigidity phase transition in granular packings," Physical Review E **60**, 6890 (1999).

[43] C.-h. Liu, S.R. Nagel, D.A. Schecter, S.N. Coppersmith, S. Majumdar, O. Narayan, and T.A. Witten, "Force fluctuations in bead packs," Science **269**, 513 (1995).

[44] D.W. Howell, R.P. Behringer, and C.T. Veje, "Stress fluctuations in a 2D granular Couette experiment: a continuous transition," Physical Review Letters **82**, 5241 (1999).

[45] D.W. Howell, R.P. Behringer, and C.T. Veje, "Fluctuations in granular media," Chaos **9**, 559 (1999).

[46] J.F. Peters, M. Muthuswamy, and A. Tordesillas, "Characterization of force chains in granular material," Physical Review E **72**, 041307 (2005).

[47] A. Smart, and J.M. Ottino, "Granular matter and networks: three related examples," Soft Matter **4**, 2125 (2008).

[48] D.M. Mueth, H.M. Jaeger, and S.R. Nagel, "Force distribution in a granular medium," Physical Review E **57**, 3164 (1998).

[49] A.R.T. van Eerd, W.G. Ellenbroek, M. van Hecke, J.H. Snoeijer, and T.J.H. Vlugt, "Tail of the contact force distribution in static granular materials," Physical Review E **75**, 060302 (2007).

[50] A.R.T. van Eerd, B.P. Tidhe, and T.J.H. Vlugt, "Numerical study of the force network emsemble," Molecular Simulation **35**, 1168 (2009).

[51] C.S. O'Hern, S.A. Langer, A.J. Liu, and S.R. Nagel, "Force distributions near jamming and glass transitions," Physical Review Letters **86**, 111 (2001).

52. L.E. Silbert, D. Ertas, G.S. Grest, T.C. Halsey, and D. Levine, "Analogies between granular jamming and the liquid-glass transition," Physical Review E **65**, 051307 (2002).

53. E.I. Corwin, H.M. Jaeger, and S.R. Nagel, "Structural signature of jamming in granular media," Nature **435**, 1075 (2005).

54. F. da Cruz, S. Emam, M. Prochnow, J. Roux, and F. Chevoir, "Rheophysics of dense granular materials: Discrete simulation of plane shear flows," Physical Review E **72**, 021309 (2005).

55. K.J. Dong, R.Y. Yang, R.P. Zou, X.Z. An, and A.B. Yu, "Critical states and phase diagram in the packing of uniform spheres," Europhysics Letters **86**, 46003 (2009).

56. A.J. Liu, and S.R. Nagel, "Jamming is not just cool any more," Nature **396**, 21 (1998).

57. M. van Hecke, "Jamming of soft particles: geometry, mechanics, scaling and isostaticity," Journal of Physics: Condensed Matter **22**, 033101 (2010).

58. C.S. O'Hern, S.A. Langer, A.J. Liu, and S.R. Nagel, "Random packings of frictionless particles," Physical Review Letters **88**, 075507 (2002).

59. C.S. O'Hern, L.E. Silbert, A.J. Liu, and S.R. Nagel, "Jamming at zero temperature and zero applied stress: The epitome of disorder," Physical Review E **68**, 011306 (2003).

60. T.S. Majmudar, M. Sperl, S. Luding, and R.P. Behringer, "Jamming transition in granular systems," Physical Review Letters **98**, 058001 (2007).

61. A.J. Liu, and S.R. Nagel, "The jamming transition and the marginally jammed solid," Annual Review of Condensed Matter Physics **1**, 347 (2010).

62. L.E. Silbert, "Jamming of frictional spheres and random loose packing," Soft Matter **6**, 2918 (2010).

63. E. Aharonov, and D. Sparks, "Rigidity phase transition in granular packings," Physical Review E **60**, 6890 (1999).

64. M.P. Ciamarra, and A. Coniglio, "Jamming at zero temperature, zero friction, and finite applied shear stress," Physical Review Letters **103**, 235701 (2009).

Tables:

Table 1. Physical parameters and conditions used in the present work

Parameter	Value	Units
Young's modulus (p, w)	2.5×10^{6}	$\pi\rho dg/6$
Poisson's ratio (p, w)	0.3	-
Sliding friction coefficient (p-p), μ_p	0.5	-
Sliding friction coefficient (p-w), μ_w	0.3	-
Rolling friction (p-p or p-w), μ_r	0.01	d
Coefficient of restitution, ε	0.8	-
Time step	0.0001	$\sqrt{d/g}$
Scaled stiffness, k^*	$3\times10^{2} - 2.5\times10^{5}$	-
Elastically scaled stress, σ*	$6\times10^{-6} - 0.3$	-
Kinetically scaled stress, σ'	$6\times10^{-2} - 7.5\times10^{4}$	-

Note: d is the maximum particle diameter, g (=9.81ms^{-2}) is the magnitude of $\boldsymbol{g}$, and ρ_p is the density of particles.

Figure captions

FIG. 1. Annular shear cell geometry: (a), the section selected for simulating the shear cell under applied normal pressure and shear velocities on platens; and (b), snapshot of particles under shearing between platens.

FIG. 2. Variation of elastically scaled applied stress (σ^*) with packing fraction (ν) for different values of scaled stiffness.

FIG. 3. Variation of kinetically scaled applied stress (σ') with packing fraction (ν) for different values of scaled stiffness.

FIG. 4. Regime map in the parametric space of: (a), (σ^*, k^*); and (b), (σ', k^*). The phase boundary between the quasi-static and intermediate regimes is determined in Fig. 2. The phase boundary between the intermediate and inertial regimes is determined in Fig. 3.

FIG. 5. Networks of scaled forces ($f = F_n/\langle F_n \rangle$) and the corresponding average coordination number and packing fraction when $k^*=3\times10^2$ for different σ^*: (a) 3×10^{-4}; (b) 3×10^{-3}; (c) 6×10^{-3}; (d) 1.5×10^{-2}; (e) 3×10^{-2}; (f) 6×10^{-2}; (g) 0.15; (h) 0.3.

FIG. 6. Networks of large scaled forces ($f >1$) and the corresponding average coordination number and packing fraction when $k^*=3\times10^2$ for different σ^*: (a) 3×10^{-4}; (b) 3×10^{-3}; (c) 1.5×10^{-2}; and (d) 0.15. The scale of all sub-figures is shown at the bottom.

FIG. 7. Probability density distributions of the scaled normal forces ($f = F_n/\langle F_n \rangle$) for different σ^* when: (a) $k^*=2.5\times10^5$; and (b) $k^*=3\times10^2$. Quasi-static/intermediate and intermediate/inertial phase boundaries are marked as B_{qi} and B_{ii}, respectively. The solid and dashed lines stand for the force

distributions obtained by Mueth et al [41] and van Eerd [42], respectively. The insets show the variation of the average contact force ($<F_n>$) with σ^*.

FIG. 8. Variation of the power index *n* in Eq. 3 with packing fraction ν for different scaled stiffness. Note that all the points on the quasi-static/intermediate regime boundary (highlighted as 'boundary points') have the *n* values close to 1.1.FIG. 9. Variation of coordination number with: (a), packing fraction ν; (b), elastically scaled applied stress σ^*; and (c), kinetically scaled applied stress σ' for different scaled stiffness. The vertical line in the main panel of (a) corresponds to the critical packing fraction of 0.58. The inset shows the scaling between CN-CN_0 and ν-ν_0 with the dotted curve standing for the best fit given in Section 3.4.

Figures

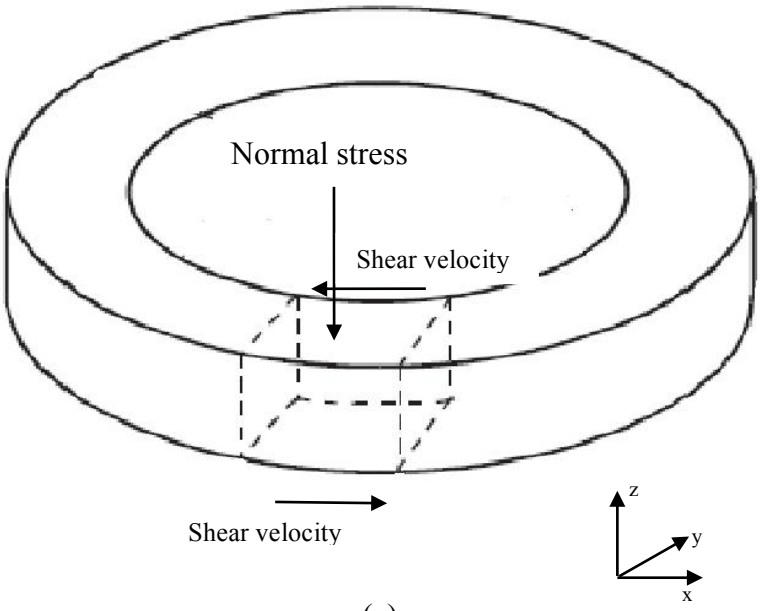

(a)

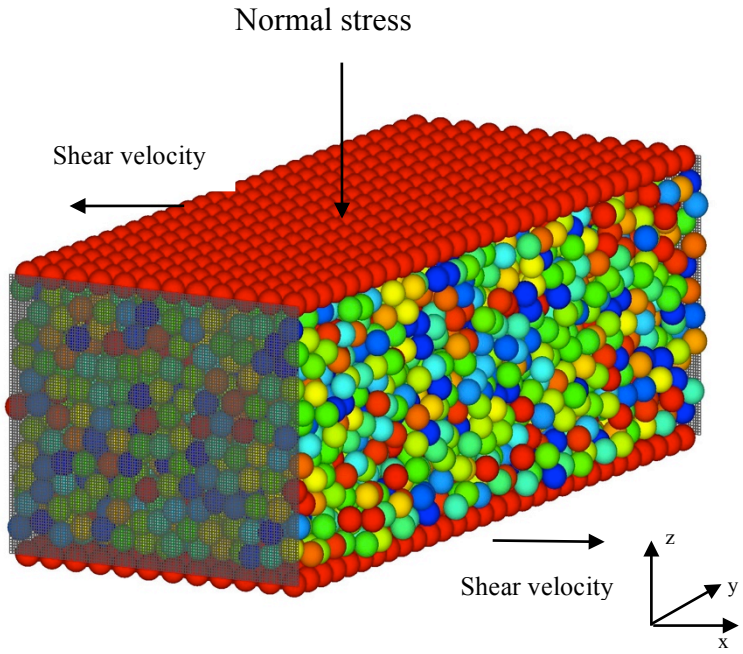

(b)

FIG. 1. Annular shear cell geometry: (a), the section selected for simulating the shear cell under applied normal pressure and shear velocities on platens; and (b), snapshot of

particles under shearing between platens.

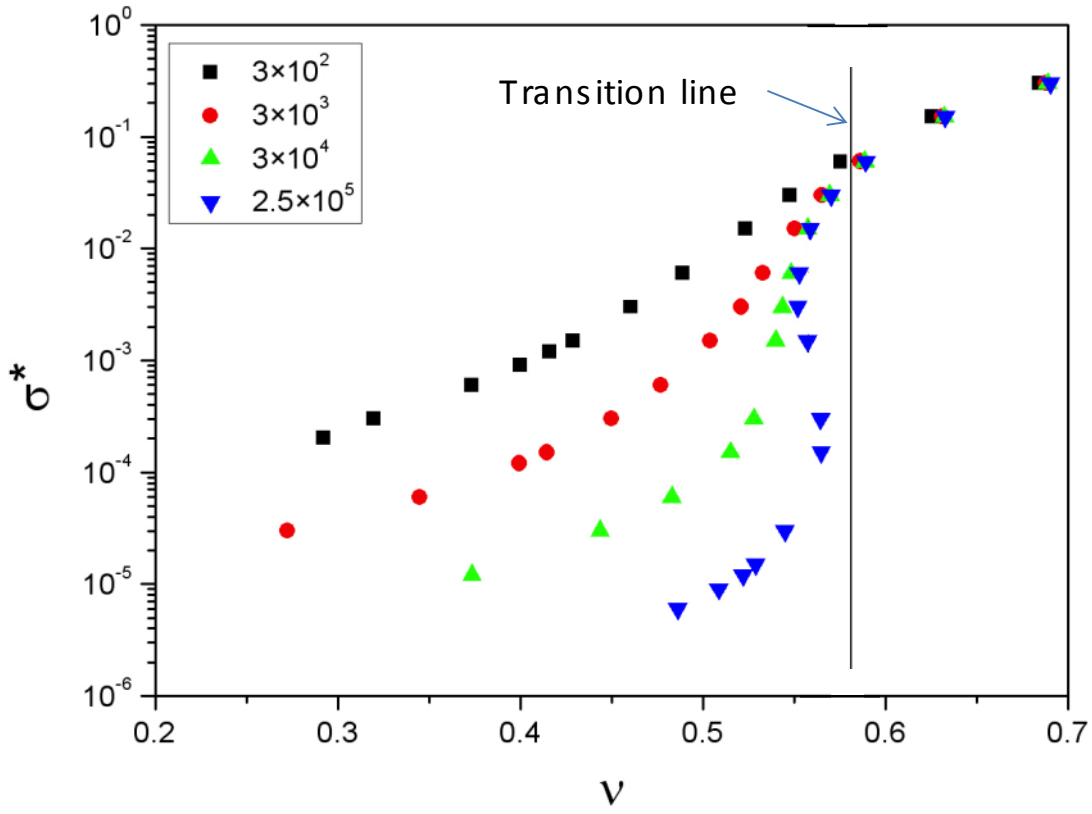

FIG. 2. Variation of elastically scaled applied stress (σ*) with packing fraction (ν) for different values of scaled stiffness.

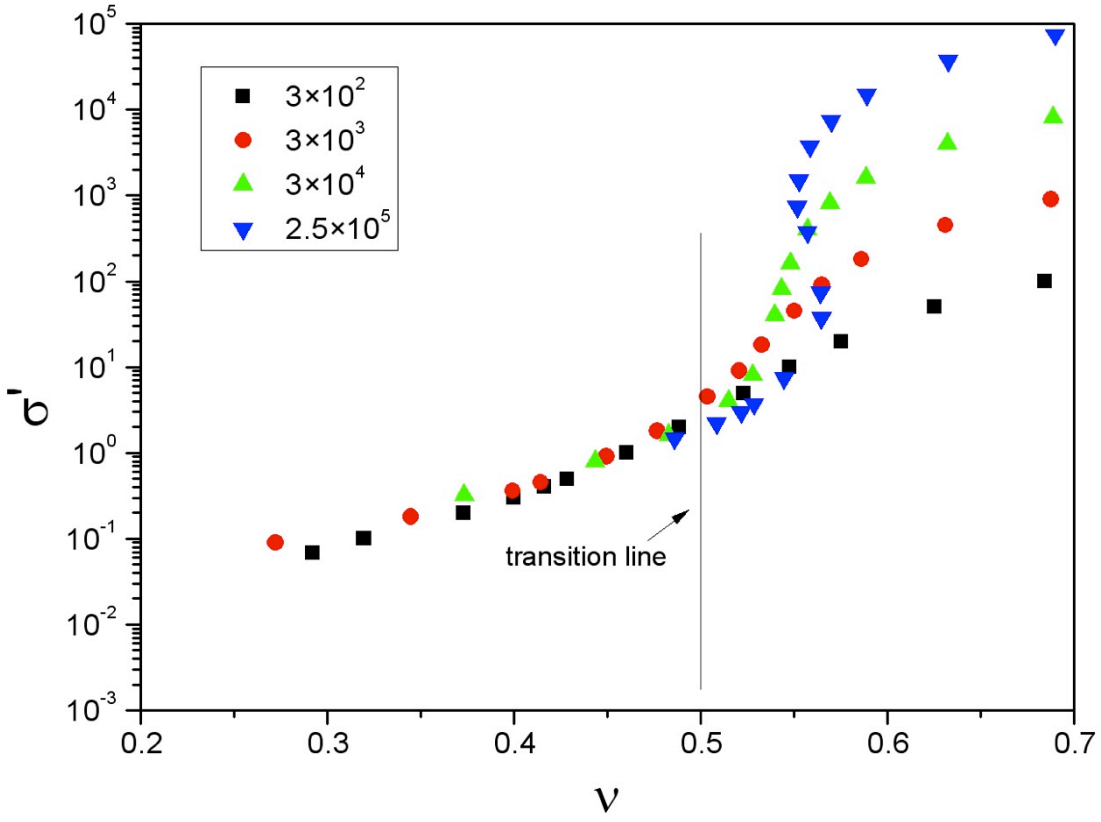

FIG. 3. Variation of kinetically scaled applied stress (σ') with packing fraction (ν) for different values of scaled stiffness.

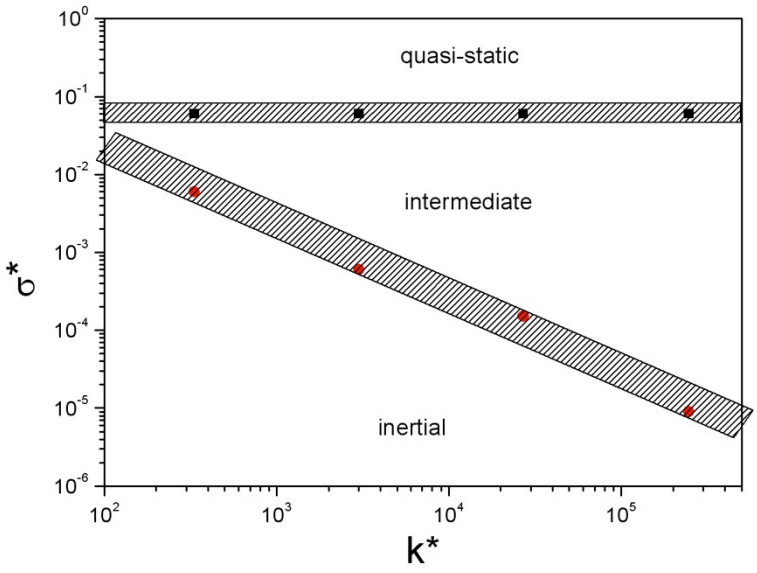

(a)

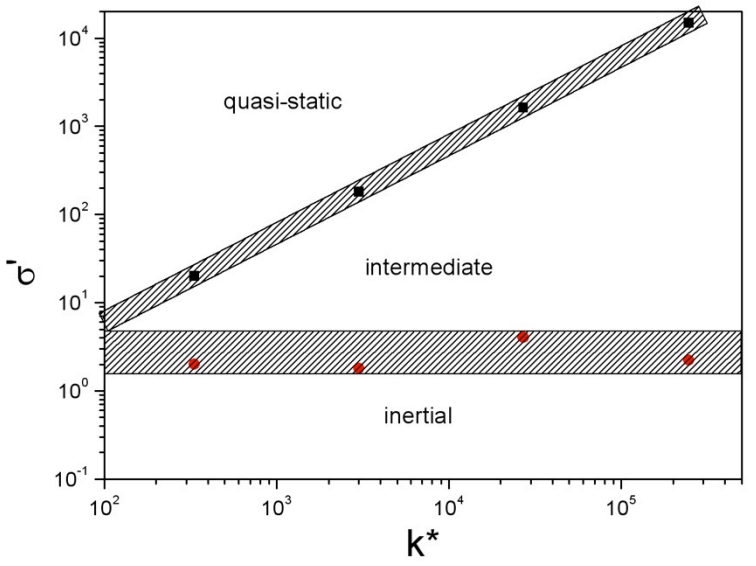

(b)

FIG. 4. Regime map in the parametric space of: (a), (σ*, *k**); and (b), (σ', *k**). The phase boundary between the quasi-static and intermediate regimes is determined in Fig. 2. The phase boundary between the intermediate and inertial regimes is determined in Fig. 3.